Chapter 4

Description of the experiment

The first section of this chapter gives a brief description of the LEP collider with emphasis on the determination of the beam energy, which is a source of systematic uncertainty for the M_{W} measurement. The second section describes the characteristics of the ALEPH detector that are relevant for the analysis. At the end, the event reconstruction and simulation is discussed, including a review of the tracking and energy flow algorithms used in ALEPH.

4.1 The LEP collider

The Large Electron Positron collider [75] was an $\mathrm{e}^+\mathrm{e}^-$storage ring of 26.7 km of circumference sited at the European Centre for Particle Physics (CERN) in Geneva (Switzerland), in operation from 1989 to 2000. It was located in a tunnel nearly horizontal (with a tilt of 1.42%, for geological reasons) at a depth between 80 and 137 m, under the French and Swiss territories (see Fig. 4.1). It has been the largest collider of this type in the world.

The LEP ring consisted of eight arcs alternating with eight straight sections. The beams were formed by four or eight bunches of electrons and positrons, defining two different working modes. Bunches were accelerated in opposite directions and crossed in eight or sixteen points, in the cases of four or eight bunches respectively. Collisions were only allowed in the four points were the experiments (ALEPH, DELPHI, L3 and OPAL) were sited. In the other points, collisions were avoided by means of a system of electrostatic separators. Bunch crossings occurred every 22 μs (11 μs) for four (eight) bunches modes respectively.

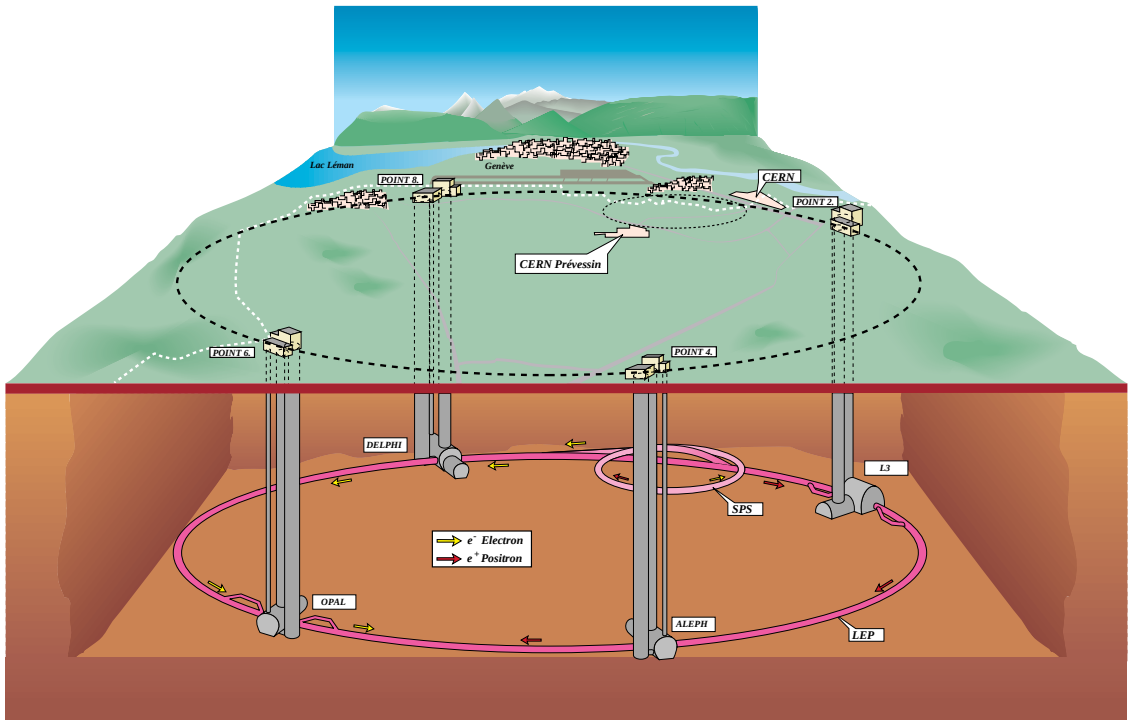

Figure 4.1: View of the LEP ring and the four interaction points.

The LEP injection chain is shown in Fig. 4.2. It started with the Linear Accelerator (LINAC) which accelerated electrons and positrons in two stages. The electrons were first accelerated up to 200 MeV. Part of these electrons were used to produce positrons by collisions with a fixed target of tungsten and the rest, together with the positrons, were accelerated up to 600 MeV. These two first linear accelerations constitute the LEP Linear Injector (LIL). Then, the particles were inserted into a small (0.12 km of circumference) storage ring, the Electron Positron Accumulator (EPA), where they were split in bunches and accumulated until the beam achieve $\sim 10^{10}$ particles. From there, the bunches were inserted in the Positron Synchrotron (PS) storage ring where they acquire an energy of 3.5 GeV. Afterwards, the particles were injected into the Super Proton Synchrotron storage ring (SPS) reaching an energy of 20 GeV. Finally, electrons and positrons were injected into the LEP main ring and accelerated up to the energy of collision.

In circular e^+e^- colliders the maximum beam energy is limited by synchrotron radiation, which is proportional to E^4/R, with E being the particle energy and R the radius

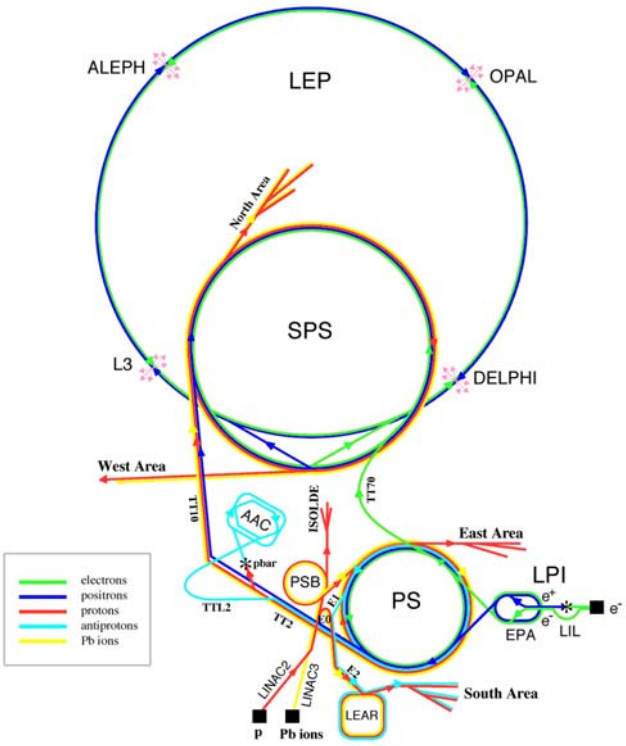

Figure 4.2: Scheme of the LEP injectors and accelerators.

of curvature. This loss of energy has to be compensated with a continuous energy supply from cavities of radio-frequency (RF), that must provide the extra-acceleration.

The LEP programme comprised two phases. In the first phase (LEP1, finished in 1995), the LEP machine was operated at the peak of Z^0 production ($\sqrt{s} \sim 91\,\mathrm{GeV}$), with luminosities at the level of $10^{31}\,\mathrm{cm}^{-2}\mathrm{s}^{-1}$. Around four million visible Z^0 decays were recorded per experiment.

The LEP2 programme started in summer 1996, when collisions at a centre-of-mass energy above the W pair production threshold ($\sqrt{s} \sim 161\,\mathrm{GeV}$) were reached for the first time in an e^+e^- accelerator. Later that year the energy was already increased to 172 GeV. In order to achieve this energy compensating for the increased synchrotron radiation, new niobium superconducting RF cavities had to be installed, partially replacing the old room temperature copper cavities. During 1997, e^+e^- collisions were produced at $\sqrt{s} = 183\,\mathrm{GeV}$ and during 1998 189 GeV were achieved by the installation of more superconducting cavities. In 1999, the centre-of-mass energy was increased gradually to

196, 200 and 202 GeV, and in 2000 to 205 and 207 GeV. This latter effort of increasing the energy of the collisions had an important impact in the final exclusion limit on the mass of the SM Higgs boson from LEP [2].

Table 4.1 summarises the integrated luminosity provided during LEP2 to the ALEPH detector for every particular $\sqrt{s}$. The total integrated luminosity per experiment was about 690 pb^{-1}.

$< E_{cm}(GeV) >$	Denomination	$\int \mathcal{L}dt(pb^{-1})$
172.09	172	10.650
182.655	183	56.812
188.60	189	174.200
191.584	192	28.931
195.519	196	79.857
199.516	200	86.277
201.625	202	41.893
204.86	205	81.640
206.53	207	133.650

Table 4.1: Integrated luminosities recorded by ALEPH at each $\sqrt{s}$ above the $\mathrm{W^+W^-}$ production threshold

4.1.1 Determination of the LEP centre-of-mass energy

At LEP, the centre-of-mass energy is used to constraint the measured jet and particle momenta, and hence it sets the absolute energy calibration of the event reconstruction. Therefore, the uncertainty introduced in the M_{W} measurement by direct reconstruction is given by $\Delta M_{\mathrm{W}}/M_{\mathrm{W}} \sim \Delta E_{beam}/E_{beam}$.

During LEP1, E_{beam} was measured directly at the operating energy with high precision, which allowed a very good determination of the Z mass and width. The method used is called resonant depolarisation (RD) [78]. It makes use of the non-negligible transverse beam polarisation appearing at circular accelerators, due to the interaction of the electrons with the magnetic field (Sokolov-Ternov effect [79]). The transverse spin precesses with a frequency that can be predicted with a very high accuracy as a function of the beam energy:

$$\nu = \frac{g_e - 2}{2} \frac{E_{beam}}{m_e c^2} = \frac{E_{beam}(\text{GeV})}{0.4406486(1)} \tag{4.1}$$

where m_e is the electron mass and $(g_e - 2)/2$ the gyromagnetic constant. This relation needs to be corrected for small imperfections because depolarisation takes place over many thousand turns of the beams.

To measure the spin precession, an exciting field perpendicular to the beam axis is provided to the electrons. When the frequency of the exciting field satisfies a certain relation with the frequencies of precession and revolution, the spin rotations add up coherently from turn to turn and a resonance appears. From the measurement of the frequency of resonance, E_{beam} can be measured to an accuracy of $\sim 0.2\,\text{MeV}$. However, only two calibrations per week were in practice feasible, and the extrapolation between them was affected by uncertainties like the status of RF cavities, temperature or humidity, etc. The final precision an the measurement was at the level of $\sim 2\,\text{MeV}$.

Unfortunately, at LEP2 this method could not be applied directly. The new frequencies of revolution required did not allow to observe spin precession resonances. Hence the measurement of the energy relied on the measurement of the magnetic field in several of the LEP main bend dipole magnets. Sixteen nuclear magnetic resonance (NMR) probes installed in 1996 were used. The field readings were calibrated to the beam energy measured by resonant depolarisation in the region of 41 to 61 GeV, at dedicated calibration runs during the LEP2 programme. A linear fit was used, with two free parameters, $E_{pol} = a + bE$. From this fit, the centre-of-mass energy at working runs could be predicted from the bending field measurement. The larger uncertainty on the method (20 MeV) comes from the extrapolation of the relation between bending field and energy from a beam energy of ∼60 GeV to LEP2 energies.

During the last two years of LEP2 running, two alternative methods were developed to cross-check the validity of the extrapolation [76]. The first method was based on the measurement of the frequency of the field that was needed to compensate from synchrotron radiation, that can be related with the beam energy itself. The second consisted in measuring the bending angle of the electrons after passing by a LEP dipole. The resolution of both measurements were of ∼20 MeV, and the results were in agreement with the value from the extrapolation.

A third method for cross-check is provided by the four LEP experiments by the re-

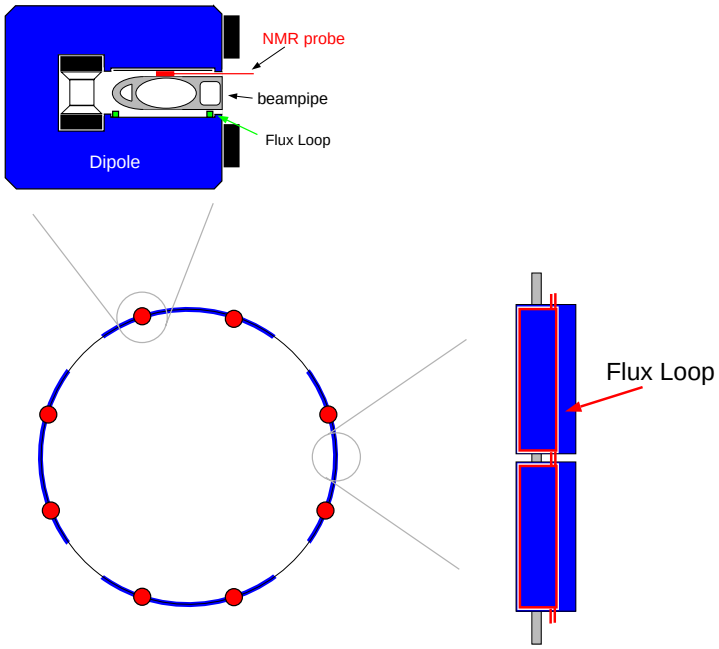

Figure 4.3: NMR probes and flux-loop used for monitoring the LEP magnetic field.

construction of radiative return events [81]. In those events an ISR photon is produced and the e^+e^- interaction occurs at a centre-of-mass energy equal to the Z mass. The comparison of the reconstructed Z peak with the precisely known Z mass is a check of the energy calibration of LEP2. The combined result from the LEP experiments is compatible with the rest of measurements: the deviation from the energy measured by the standard method is measured to be $\Delta E_{beam} = -10 \pm 27(\text{stat}) \pm 26\,\text{MeV}\,(\text{syst})$.

The energy measurement is corrected for several effects like the variation of the LEP geometry due to Earth tides, temperature effects or leakage currents from neighbourhood Geneva-Paris TGV electric trains. There are also corrections to relate the average energy to the collision energy at each interaction point, in particular due to the exact accelerating RF configuration. All of these effects have been rather well understood at LEP1 [78], and contribute a total additional uncertainty below 10 MeV [77] at LEP2.

The beam energy is determined with an average precision of 25 MeV [77] for the data taken in LEP2, about 10 times larger than the uncertainty at LEP1.

4.2 The ALEPH detector

The ALEPH detector [71] (Apparatus for LEp PHysics) was one of the four multi-purpose detectors installed in the LEP collider, together with DELPHI [72], L3 [73] and OPAL [74]. The main overall objectives of the ALEPH design were the precise measurement of the parameters of the electroweak Standard Model, testing QCD at large Q^2 and searching for the Higgs boson and for new physics, like super-symmetric particles. The detector was conceived to provide a good hermeticity with a good track resolution and fine calorimetric granularity.

ALEPH [82] was located at the experimental point number four (next to Echenevex, in France) in a cavern 143 m below the ground surface. It was a cylinder of 12 m diameter by 12 m length weighting about 4000 tons, positioned around the beam pipe, which was a tube of 10 cm of radius that forms part of the accelerator. ALEPH covered 95% of the solid angle around the central interaction point.

The ALEPH reference system is defined as follows. The origin is the theoretical beam crossing point; the z direction is along the beam line, positive in the direction followed by the electrons, thereby slightly different from the local horizontal direction due to the fact that the accelerator is slightly tilted. The positive x direction points to the centre of LEP, and is horizontal by definition. The positive y direction is orthogonal to z and x pointing upwards, and deviates 3.5875 mrad from the local vertical direction.

The detector consists of independent and modular sub-detectors arranged in layers, each one specialised in a different task. There were two main type of sub-detectors: tracking devices, which allow to reconstruct the trajectories of charged particles and to classify them using the ionisation left in the detectors, and calorimeters (electromagnetic and hadronic) which gave a measurement of the energy of the particles, being also the only detectors capable to give information of the direction of neutral particles. Muons were identified using the muon chambers and/or the final planes of the hadronic calorimeter. Specialised detectors situated at low angle give a precise measurement of the luminosity.

Some other sub-detectors monitored the instantaneous luminosity and the background. Finally, the trigger and data acquisition systems were used to decide when to read the events and to record them, respectively. A brief description of these devices follows, mainly stressing their performances [83]. A detailed and complete description can be found in [71, 82].

Main detectors

A particle *flying* from the central interaction point across ALEPH encountered the following sub-detectors (see Fig. 4.4):

- **The Mini Vertex DETector (VDET)**: a double sided silicon strip device with two layers of strips, one parallel (z) and one perpendicular ($r\phi$) to the beam, placed around the beam pipe. It provided a very accurate vertex tagging of tracks coming from the interaction point (with $|\cos\theta| < 0.9$) with a coordinate spatial resolution of $10\,\mu$m in $r\phi$ and $15\,\mu$m in z. It played a very important role in the reconstruction of particles with very short lifetime, like the τ lepton or hadrons containing b or c quarks, through the accurate measurement of the impact parameter of their charged decay products.

- **The Inner Tracking Chamber (ITC)**: a cylindrical multi-wire drift chamber, that provided the coordinates of up to eight precise $r\phi$ points per track, with an accuracy of $150\,\mu$m per coordinate. It contributed to the global ALEPH tracking and to the triggering of charged particles coming from the interaction region.

- **The Time Projection Chamber (TPC)**: the largest tracking detector of ALEPH, was a cylindrical imaging drift chamber of 4.7 m long with 31 cm and 180 cm inner and outer radius respectively. The three coordinates of the particle trajectories were measured by the TPC. The z-coordinate was obtained from the drift time and the known drift velocity; the ϕ coordinate was calculated interpolating the signals induced on cathode pads located precisely on the sectors (the end-plate where the charged particles were collected is divided into 18 wire chambers or sectors), and the r-coordinate was given by the radial position of the pads. It provided up to 21 three-dimensional coordinate points for each charged track crossing the chamber. The single coordinate resolution was $173\,\mu$m in the azimuthal direction and $740\,\mu$m in the longitudinal direction. From the curvature of tracks, due to the presence of a magnetic field, the TPC gave a measurement of transverse particle momenta (p_T) with an accuracy of $\Delta p_T/p_T^2 = 0.6 \times 10^{-3}\,(\mathrm{GeV})^{-1}$ at 45 GeV, if used together with the ITC and the VDET. The chamber also contributed to charged particle identification through measurements of energy loss (dE/dx) derived from about 320 samples of ionisation for a track traversing the full radial range.

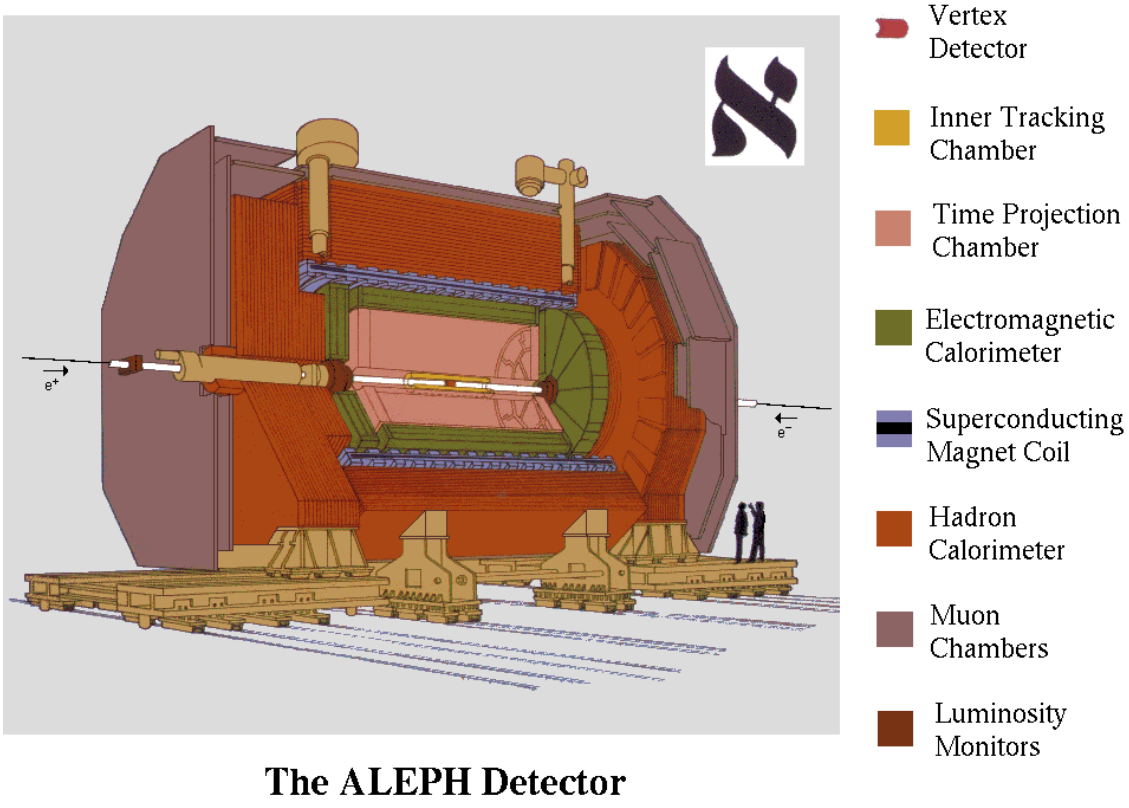

Figure 4.4: The ALEPH detector.

– **The Electromagnetic CALorimeter (ECAL)**: a sampling calorimeter that measured the energy and position of electromagnetic showers. It was longitudinally segmented in three compartments (one barrel and two end-caps). Each compartment consisted of alternating lead sheets and proportional wire chambers read out in projective towers. A granularity of about $0.9^{\circ} \times 0.9^{\circ}$ of solid angle pointing to the interaction point was obtained. The energy resolution was $\sigma(E)/E = \left(0.18/\sqrt{E}/\mathrm{GeV}\right) + 0.009$. The good position and energy resolutions lead to a good electron identification and allow to measure photon energy even in the vicinity of hadrons.

– **The Superconducting coil**: a liquid-Helium cooled superconducting solenoid. It created, together with the iron yoke, a 1.5 T axial magnetic field in the central detector. The field bended the particle directions and allowed the measurement of their momenta in the tracking detectors.

– **The Hadronic CALorimeter (HCAL)**: a sampling calorimeter longitudinally segmented as ECAL, made of layers of iron and streamer tubes, and globally rotated 1.875° with respect to ECAL in order not to superimpose the crack regions (3.4% of the solid angle for HCAL). It measured energy and position for hadronic showers and, complemented with the muon chambers, acted as a muon detector. The energy resolution for a charged pion was $\sigma(E)/E = 0.85/\sqrt{E/\mathrm{GeV}}$. The readout was performed twice: using cathode pads forming projective towers and using digital readout of the streamer tubes for muon tracking and for triggering. HCAL also provided the main support of ALEPH, the large iron structure serving both as hadron absorber and as return yoke of the magnet.

– **The MUON chambers (MUON)**: outside HCAL, formed by two double layers of limited streamer tubes which measured position coordinates of muons, the only detectable particles reaching that sub-detector. For a muon travelling through both layers of muon chambers, the direction of the track was determined with an accuracy of about 10-15 mrad.

Luminosity measurement

Precise measurements of the SM parameters require an accurate knowledge of the luminosity ($\mathcal{L}$). At LEP, $\mathcal{L}$ was measured through the rate of small-angle Bhabha scattering events ($e^+e^- \to e^+e^-$). The integrated luminosity is calculated by using the formula:

$$\int \mathcal{L}\, dt = \frac{N_{\mathrm{Bhabha}}}{\sigma_{\mathrm{Bhabha}}}, \tag{4.2}$$

where N_{Bhabha} is the number of Bhabha events and σ_{Bhabha} is their corresponding cross-section, which is theoretically computed with the programme `BHLUMI` [84] taking into account the experimental acceptance. The systematic component dominates the uncertainty in the luminosity measurement. It is at the level of the 0.1%, and it includes a theoretical uncertainty in the cross-section calculation of 0.06%.

Three different sub-detectors installed around the beam pipe provided a luminosity measurement in ALEPH:

– **The Luminosity CALorimeter (LCAL)**: a lead/wire calorimeter similar to ECAL in its operation. It consisted of two pairs of semi-circular modules placed around the beam pipe at each end of the detector. Its acceptance in polar angle

span from 45 to 160 mrad. At LEP2, it was the responsible for providing the *official* ALEPH luminosity. The luminosity measurement consisted essentially of *counting* the number of events for which there were two back-to-back deposits of energy compatible with the beam energy, which is the standard way for identifying Bhabha scattering events.

– **The SIlicon luminosity CALorimeter (SICAL)**: installed in September 1992 on each side of the interaction region. It consisted of a cylindrical calorimeter around the beam pipe with 12 silicon/tungsten layers, used to sample the showers produced by small angle Bhabha events. During the LEP1 phase, it provided the official ALEPH luminosity, since it improved the statistical precision of the luminosity measurement by sampling at smaller angles than LCAL. The systematic error on the luminosity was also reduced thanks mainly to the greater precision in the positioning of its components. At LEP2, the luminosity provided by SICAL was not used to normalise the physics processes cross-sections in ALEPH, because it was partially hidden by the masks installed to protect the central detectors from the synchrotron radiation, much higher than at LEP1. Instead, it was used to improve the ALEPH acceptance at very low angle.

– **The Bhabha CALorimeter (BCAL)**: located behind the final focus quadrupoles, consisted of a system of four modules, each of them being a sampling calorimeter made of tungsten converter sheets interspersed with sampling layers of plastic scintillator, plus a single plane of silicon strips with $r\phi$ segmentation. This plane was used to locate the shower position. BCAL gave a measurement of the instantaneous luminosity and acted as a background monitor. It was sited at very low angles, allowing high statistics at the cost of increased systematic errors. It provided a fast on-line estimation of the luminosity.

Beam monitoring

The beam conditions needed to be monitored for the optimisation of the LEP performance. The background level was monitored in ALEPH by the Small Angle Monitor of BAckground (SAMBA) positioned in front of LCAL at each end of the detector. Other devices located around the circumference of LEP, called Beam Orbit Monitors (BOM's), were used to measure the mean position and angle of the beam orbits. This information was used by LEP to optimise the beam conditions, and by ALEPH to determine the (x, y)

position of the beam spot as a starting point for off-line reconstruction of the primary vertex.

Trigger system

The purpose of the ALEPH trigger was to identify all the relevant events coming from e^+e^- annihilations and to reduce to a low level the rate of useless events: collisions of the beam with the residual gas, off-momenta beam electrons hitting the beam pipe walls, electronic noise, cosmic rays or photons radiated by bremsstrahlung. The trigger reduced the dead time in the detector and avoided the recording a large amount of useless data. The trigger system was designed to be sensitive to single particles or single jets. It produced a signal that started the event read-out, which was adjusted so that the TPC was gated at an acceptable low rate and the dead time induced by readout was negligible.

The triggering process was organised in three levels:

- **Level one trigger:** it made the decision whether to read or not all the detector elements. Its purpose was to operate the TPC at a suitable rate. The decision was taken approximately 5 μs after the beam crossing (fast decision when compared to the time between two bunch crossings, 11 μs) from pad and wire information from ECAL and HCAL, and hit patterns from the ITC. The requirement for the maximum rate of the level one trigger was a few hundred Hz. After a negative decision, the TPC was reset and kept ready for the next event, while after a positive decision the digitisation of the signals is initiated.

- **Level two trigger:** it refined the level one triggers by using the TPC tracking information to check whether the trajectories of the charged particles originate close to the interaction point. If the level one decision was not confirmed, the readout process was stopped and cleared. The decision was taken approximately 50 μs after the beam crossing (the time at which the TPC tracking information is available). The maximum trigger rate allowed for this level was about 10 Hz.

- The **Level three trigger:** it had access to the information from all detector components and it was used to reject background, mainly from beam-gas interactions and off-momentum beam-particles. It ensured a reduction of the trigger rate to 3-4 Hz, acceptable for data storage.

Data Acquisition system

The data acquisition (DAQ [85]) system allowed each sub-detector of ALEPH to take data independently. It activated the trigger system at every beam crossing and wrote the data in a storage system following every level-two *YES* decision. The DAQ also monitored and regulated continuously all the detector and electronic system.

The architecture of the system was hierarchical. Following the data and/or control flow from the bunch crossing of the accelerator down to the storage device, the following components were found:

- Timing, Trigger and Main Trigger Supervisor: synchronised the readout electronics to the accelerator and informed the Read-Out Controllers (ROC's) about the availability of the data.
- ROC's: initialised the front-end modules, read them out and format the data.
- Event Builders (EB's): built a sub-event at each sub-detector level.
- Main Event Builder (MEB): collected the pieces of an event from the various EB's and ensured re-synchronisation and completeness.
- Level three trigger: performed a refined data reduction, as already seen before.
- Main host and sub-detector computers: the main machine (an AXP cluster) initialised the complete system, collected all data for storage and provided the common services.

The data taken by the online computers was called *raw data* and was reconstructed quasi-online. In less than two hours after the data was taken, the event reconstruction and a check of the quality of the data were done, thus allowing ALEPH to have a fast cross-check of the data quality and to correct possible detector problems. That task was performed by the Facility for ALeph COmputing and Networking (FALCON) [86], three AXP processors running the full ALEPH data reconstruction programme JULIA (Job to Understand LEP Interactions in ALEPH) [87] which performed the majority of track fitting and calorimeter reconstruction needed for physics analysis. The output of JULIA provided the quality of the data taken (RunQuality) and was written in POT (Production Output Tape) data files.

Finally, the ALPHA (ALeph PHysics Analysis) [88] package can be used as an interface allowing easy access to the reconstructed physical quantities of particles such as momenta, energies, etc. This process is described in the following section.

4.3 Event reconstruction

This section briefly describes the two main processes that contribute to the reconstruction of events in ALEPH, namely the track reconstruction and the energy flow algorithm.

4.3.1 Tracking in ALEPH

The first step of the track reconstruction is grouping nearby hits in the TPC to form clusters (track segments) for which three coordinates are determined. In the ITC, three coordinates are reconstructed as well, taking into account the wire number and the difference of the arrival times of the signals to the two ends of the wire. The reconstruction of the tracks starts in the TPC by connecting track segments to determine tracks consistent with a helix hypothesis. These track candidates are then extrapolated to the inner detectors, ITC and VDET, where consistent hits are assigned. Coordinate errors are determined using the preliminary track parameters. The final track fit, based on Kalman Filter [90] techniques, uses these errors and takes into account multiple scattering effects between coordinates and the energy loss (when passing through the beam pipe and materials in the tracking detectors) in flight.

The track finding efficiency in the TPC was studied [83] using MC hadronic Z^0 events, indicating that 98.6% of tracks that cross at least four pad rows in the TPC are reconstructed successfully; the small inefficiency, due to track overlaps and cracks, is reproduced to better than 0.1% by the simulation. The efficiency of associating a vertex detector hit to an isolated track is about 94% per layer, within the geometrical acceptance. By selecting di-muon events at 45 GeV in the angular acceptance $|\cos\theta| < 0.8$, the transverse momentum resolution is $\sigma(1/p_T) = 1.2 \times 10^{-3}\,(\mathrm{GeV})^{-1}$ for the TPC alone. It improves up to $\sigma(1/p_T) = 0.6 \times 10^{-3}\,(\mathrm{GeV})^{-1}$ (already mentioned before) when VDET, ITC and TPC are used together.

4.3.2 Energy-flow determination

The energy flow algorithm [83] is an event-shape algorithm which is used in this work to analyse hadronic events.

The simplest way to determine the energy flow of an event recorded in the ALEPH detector is to make the sum of the raw energy found in all calorimetric cells without performing any particle identification. The energy resolution of this naive method is very limited:

$$\sigma(E) = 1.2\sqrt{E/\mathrm{GeV}} \tag{4.3}$$

for hadronic Z^0 decays. A better solution is the use of an energy flow reconstruction algorithm, which makes use of the track momenta and takes advantage of the photon, electron and muon identification capabilities to improve the energy resolution. A description of the energy flow algorithm follows.

A first cleaning procedure is applied to eliminate from the calculation poorly reconstructed tracks, noisy channels of ECAL and HCAL, and fake energy deposits in the calorimeter towers. This is done by requiring charged particle tracks with at least four hits in the TPC originating from within a cylinder of length 20 cm and radius 2 cm centred at the nominal interaction point and coaxial with the beam direction, reconstructed using the information of the VDET, the ITC and the TPC.

Afterwards, the charged particle tracks are extrapolated to the calorimeters, and groups of topologically connected tracks and clusters (so-called *calorimeter objects*) are formed (some of the calorimeter objects do not have any associated track). To avoid double-counting, the calorimetric energy already associated to tracks is removed from the calorimeter objects.

From the original list of calorimeter objects, those identified as electrons, muons or photons are removed. Then, any object remaining in the calorimeter list should be charged or neutral hadron. Those containing charged particle tracks coming from the nominal interaction point or belonging to a reconstructed V^0 (long-lived neutral particles decaying into two oppositely-charged particles) are counted as charged energy. They are assigned the mass of a pion.

For the rest of objects (that should correspond to neutral hadrons) a specific identification is not done. The component from the electromagnetic calorimeter is scaled by the ratio of the calorimeter's response to electrons and pions. If this sum exceeds the energy

of any remaining charged particle tracks, and the excess is both larger than the expected resolution on that energy when measured in the calorimeters, and greater than 500 MeV, then the object is kept as a neutral hadronic particle.

As a result of this algorithm, a set of *energy flow objects* (electrons, muons, photons, charged or neutral hadrons) is obtained, all of them characterised by their energies and momenta. All the clusters found in the luminosity monitors, where no particle identification is available, are added to this list. Neutrinos, which escape of the detector, are indirectly detected by the presence of missing energy in the event.

The energy resolution of the energy flow algorithm was studied by reconstructing the peak of the invariant mass of the Z^0 from hadronic decays. The resulting energy resolution could be parametrised as [83]:

$$\sigma(E) = (0.59 \pm 0.03)\sqrt{E/\mathrm{GeV}} + (0.6 \pm 0.3)\ \mathrm{GeV}, \tag{4.4}$$

representing a big improvement with respect to what was obtained from the calorimeters alone (equation (4.3)).

4.4 The event simulation

The different physics analyses make use of MC simulated events in order to evaluate background contaminations, compute acceptances and efficiencies and, in general, compare the theoretical models to the experimental results. In this particular work, MC events are also used as reference to fit the invariant mass distribution. The chain followed to produce simulated events is:

- **Generation of event kinematics:** the different particle four-momenta are generated according to the different physics processes, as described in Section 3.1. In ALEPH, the different MC codes to generate each physics process are unified through a common interface: `KINGAL` [91].

- **Simulation of the detector response:** done by using a `GEANT` [92] based programme (`GALEPH` [93]) where all the information about the geometry and materials involved in the experimental setup are described. For the tracking simulation, the primary long-lived particles are followed through the detector. Secondary particles are also produced by interaction with the detector material. Bremsstrahlung,

Compton scattering and ionisation are some of the processes simulated. `GEANT` and `GHEISHA` [94] are used to simulate the electromagnetic and nuclear interactions of particles with matter respectively. The energy depositions are converted into measurable electrical signals.

- **Reconstruction:** the same programme (JULIA) used for the real data is used for the simulated events. Therefore, the output of all the simulation processes has the same format as that of the real data.

Monte Carlo generators

Different MC packages are used to generate the different physics processes observed by ALEPH. A brief description of the MC programs used to simulate the signal and background events in this analysis follows.

- `KORALW` **[14]** W^+W^- **signal Monte Carlo**:
  This programme (version 1.53.2) includes multi-photon initial state radiation with finite photon transverse momentum via Yenni-Frautschi-Suura exponentiation [17], final state radiation via `PHOTOS` [18], and Coulomb correction [8]. It can generate `CC03` diagrams (Fig. 2.1), or include four fermions diagrams computed with the `GRACE` package [95]. Loose cuts are applied at the generator level on the outgoing electron angle of the fermion-anti-fermion pair invariant masses in order to avoid regions of phase space with poles in the cross-section. The W^+W^- events produced in these regions would in any case be rejected by the selection cuts. The `JETSET` package [96] takes care of gluon radiation and hadronisation. BEC and CR effects are not included by default.

- **Monte Carlo's of background processes**:
  Annihilation into quark pairs, $e^+e^- \rightarrow q\bar{q}$, are simulated with `PYTHIA/HVFL05/KK2F02` [96]. Di-leptons final states are generated with `KORALZ` [99] and `UNIBAB` [100]. `PYTHIA` and `KORALW` are also used for various processes leading to four fermion final states such as ZZ and Ze^+e^-. This last process is simulated with the electrons generated to smaller angles than the acceptance cut used in the production of the four fermion events.

Chapter 5

Event selection and reconstruction

The first step in the M_{W} measurement is the selection of the $\mathrm{W}^+\mathrm{W}^-$ signal events among the data recorded by ALEPH. Once the events are selected, the invariant masses of the W bosons have to be reconstructed from the collection of observed energy flows. These two steps of the analysis are described in this chapter.

5.1 Event selection

This section starts with a summary of the characteristics of the signal and the potential backgrounds. Afterwards, the selection process is described in two phases: the so-called preselection and a second stage based on the use of a neural network.

5.1.1 Signal and background characteristics

Fully hadronic events are characterised by the presence of at least four jets, which provide a large multiplicity and a spherical topology. The missing energy in the event is small, so the total energy is close to the LEP centre-of-mass energy. Several physics processes *simulate* these characteristics, and consequently can be selected as hadronic $\mathrm{W}^+\mathrm{W}^-$ events. These potential background channels are $e^+e^- \to q\bar{q}$, ZZ, Ze^+e^- and leptonic or semileptonic $\mathrm{W}^+\mathrm{W}^-$ events. The cross-sections of these processes are listed in Table 5.1.

The $e^+e^- \to q\bar{q}$ process has a cross-section much larger than that of the signal, but it is the background with a more distinct topology. Over 50% of $\mathrm{q\bar{q}}$ events are characterised by radiative return to the Z resonance with a photon escaping through the beam pipe,

Channel	$\sigma(\times BR)(pb)$
Signal	8.13
$e^+e^- \to \mathrm{q\bar{q}}$	101.5
$e^+e^- \to \mathrm{Z}e^+e^-$	8.01
Semileptonic $\mathrm{W^+W^-}$events	7.74
$e^+e^- \to ZZ$	2.18
Fully leptonic $\mathrm{W^+W^-}$ events	1.84

Table 5.1: Cross-section of the signal and background processes at $\sqrt{s} = 189\,\mathrm{GeV}$. The cross-section for $\mathrm{W^+W^-}$ processes is multiplied by the branching ratio of the given final state.

and hence have a large amount of missing energy. In addition, most of the $\mathrm{q\bar{q}}$ events have a longitudinal two-jet structure. Nevertheless, a fraction of them can fake the typical four jet topology of hadronic $\mathrm{W^+W^-}$ events by emission of gluon jets or by artifacts of the jet clustering procedure.

ZZ events in which both Z bosons decay to a pair of quarks have a topology very similar to that of the signal. The only way of rejecting this background is by applying an anti-b tagging, making use of the fact that no b-jets can be present in the decay of a W boson. Ze^+e^- events could in principle contribute if the two electrons are tagged as jets by emission of radiation, by quark-gluon emission or any combined effect.

Semileptonic $\mathrm{W^+W^-}$ decays are characterised by one energetic lepton that is usually isolated from the two jets. Also a large amount of missing energy is present due to the neutrino. Fully leptonic $\mathrm{W^+W^-}$ events are characterised by two energetic leptons and a large amount of missing energy. Non-hadronic $\mathrm{W^+W^-}$ channels may pass the preselection but are effectively removed from the sample at the neural network stage.

The following subsections describe the two steps of the event selection chain: the preselection and the neural network selection.

5.1.2 Preselection

The preselection is designed to discard those events that are very clearly not signal-like. Requirements are applied to several variables in turn, and events are removed at each stage. The criteria used are as follows:

- "`CLASS16`". At the event reconstruction phase, events are classified according to different criteria to simplify later analysis. `CLASS16` was originally designed to select hadronic events at LEP1, but it can equally be applied for hadronic W^+W^- events. `CLASS16` events have at least five *good* charged tracks within the detector acceptance, and the total energy of all charged tracks is at least 10% of the LEP centre-of-mass energy. A *good* track is defined as follows: it must have at least four hits in the TPC and come from a region close to the interaction point that is defined by a cylinder of radius 2 cm and length 20 cm; the polar angle of the track must satisfy $|\cos\theta < 0.95|$. The `CLASS16` requirement removes low multiplicity background events such as fully leptonic W^+W^- events, but also events not originating from e^+e^- collisions such as beam to gas, beam to beam pipe interactions and cosmic rays.

- $|p_z| < 1.5\,(M_{vis} - M_Z)$, where p_z is the z component of the total momentum of all the energy flow objects observed in the event and M_{vis} is the total invariant mass of all energy flow objects. This criterion removes radiative returns to the Z in $q\bar{q}$ events.

- $y_{34} > 0.001$. y_{34} is the value of the jet clustering parameter y_{cut} where the transition between three and four jets takes place. This requirement selects events which look more like four jet events, rather than the two and three jet like $q\bar{q}$ events. At this stage the events are forced into four jets using the `DURHAM` algorithm as described in Section 5.2.1.

- The fraction of the jet energy due any single charged object of each jet must be less than 90% of the total energy in the jet. This requirement rejects semileptonic W^+W^- events, which often contain a highly energetic isolated charged lepton that has been classified as a jet.

- If a photon candidate is found in one jet, the energy belonging to the candidate plus that of any particle within 1° from it must be less than 95% of the total energy in the jet. This requirement rejects events in which an initial state radiation photon is produced within the detector acceptance.

The cumulative effects of the preselection criteria on the data sample corresponding to $\sqrt{s} = 189\,\text{GeV}$ are shown in Table 5.2. The expectations from signal and background MC are also listed. There is an excess of observed events after the `CLASS16`stage, due to

processes which are not included in the MC expectation. Those processes (like $\gamma\gamma$, $\tau^+\tau^-$ and Bhabha scattering) do not contribute to the final selected sample [109].

Selection Criteria	Efficiency (%)	Purity (%)	Events Expected	Events Observed
`CLASS16`	100.0	7.0	18972	21724
$\lvert p_z\rvert < 1.5\,(M_{vis} - \mathrm{M_Z})$	99.6	12.6	10546	10849
$y_{34} > 0.001$	98.6	22.0	5991	5955
$\max\,(E_{ch}/E_{jet}) < 0.9$	98.3	23.7	5545	5451
$\max\,(E_{em}/E_{jet}) < 0.95$	97.4	37.4	3485	3293

Table 5.2: Performance of the preselection criteria, applied cumulatively to `CLASS16` events for the $\sqrt{s} = 189\,\mathrm{GeV}$ data and MC.

5.1.3 Neural network selection

After preselection, a neural network (NN) [101, 102] is used to improve the purity of the selected sample. In general, neural networks have a better performance than other multivariate techniques because variables are combined in a non-linear way, allowing to take into account correlations between them.

The NN used is a feed-forward network (there are no connections between the neurons in the same layer). The output is a number that varies between zero and unity. The higher the number the more likely an event is to be a signal event. Before the NN can be used to separate signal from background, the weights of the connections have to be determined. Samples of MC (signal and background) events are used to perform the training.

The variables provided as NN input need to have discriminating power. Studies have shown that good performance can be obtained with the use of 14 different variables [102], related to three different levels of the event structure: global properties, properties of individual jets, and $\mathrm{W^+W^-}$ kinematics. These variables are listed in Table 5.3.

Since the training of the neural network is performed using MC events, it is important that there is good agreement between data and MC, particularly in those variables that are used as input. The agreement has been checked extensively in ALEPH [103].

The output of the NN is shown in Fig. 5.1 for $\sqrt{s} = 189$ and $207\,\mathrm{GeV}$, data and MC. It can be seen that the output peaks at zero and unity providing good separation

Global Variables	1	Thrust
	2	Sphericity
	3	Missing Energy
Jet Properties	4	Maximum electromagnetic energy fraction of a jet in any 1 degree cone
	5	Maximum charged track energy fraction of a jet
	6	Minimum number of charged particles in a jet
W^+W^- Kinematics	7	Sum of the four smallest inter-jet angles
	8	Angle between 2nd and 3rd jets (ordered by decreasing energy)
	9	Maximum jet energy
	10	2nd minimum jet energy
	11	Minimum jet energy
	12	2nd minimum jet mass
	13	Minimum jet mass
Flavour Tagging	14	Probability of an event to be a light quark (uds) event based on impact parameter significance of charged particles in the event (anti b-tag)

Table 5.3: The fourteen variables used as input to the neural network.

between signal and background events. There is reasonable agreement between data and MC. To perform the separation, a cut in the output value has to be chosen. Dedicated studies [104] showed that the result of the analysis is stable in a wide range of choices. A cut at 0.3 is used in this analysis.

The NN is trained separately with MC at each centre-of-mass energy. The performance is shown in Table 5.4. Table 5.5 shows the individual contributions of all the background channels in the final selected sample, as expected from MC at $\sqrt{s} = 189\,\mathrm{GeV}$.

The event selection process described has been proved not to bias the measured W mass by having a mass dependent efficiency, by using several MC samples generated with different W masses [104].

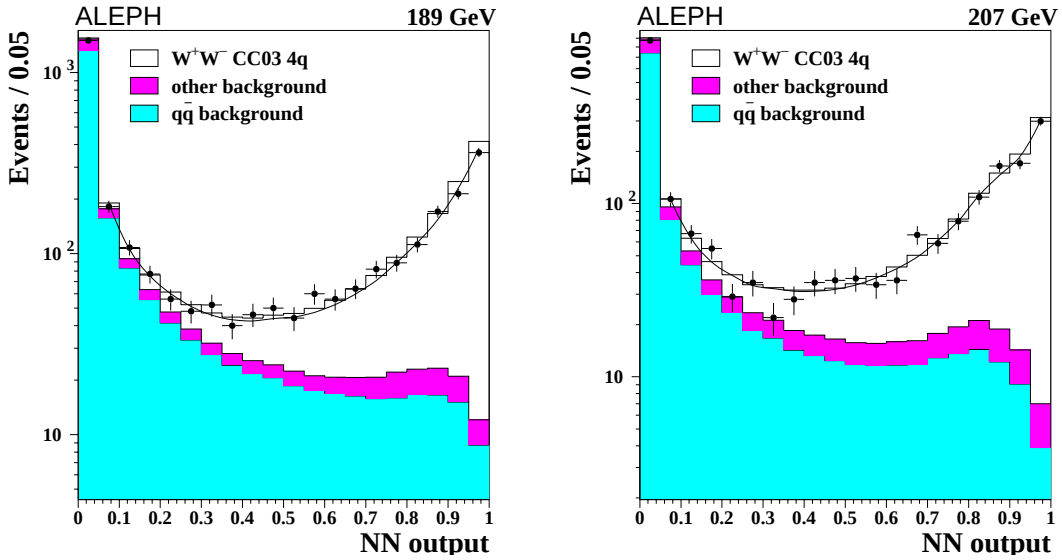

Figure 5.1: Output of the neural network, showing the discrimination between signal and background events, at $\sqrt{s} = 189$ and 207 GeV.

$\sqrt{s}$ (GeV)	$\mathcal{E}$ (%)	$\mathcal{P}$ (%)
183	79.7	82.4
189	80.1	83.8
192	79.8	85.8
196	80.4	85.7
200	80.2	85.0
202	79.8	85.4
205	79.8	85.2
207	79.5	85.4

Table 5.4: Efficiency and purity after preselection and NN cut.

5.2 Event reconstruction

Once W^+W^- candidate events have been selected, the individual W masses have to be reconstructed. First, the energy flows observed must be associated into jets, and then the jets have to be associated according to the W from which they decay. The invariant

Channel	Contribution (%)
Signal	83.8
$e^+e^- \to \mathrm{q\bar{q}}$	13.6
$e^+e^- \to ZZ$	1.97
$e^+e^- \to \mathrm{Z}e^+e^-$	0.10
Semileptonic $\mathrm{W^+W^-}$ events	0.54
Leptonic $\mathrm{W^+W^-}$ events	< 0.01

Table 5.5: Expected composition of the selected sample at $\sqrt{s} = 189\,\mathrm{GeV}$.

masses of the two W bosons is then given by

$$M_{inv}^2 = (E_1 + E_2)^2 - (\vec{p}_1 + \vec{p}_2)^2 \ , \tag{5.1}$$

where the sums are carried out over the two jets assigned to each W boson. The whole process is called event reconstruction, and each of the steps are described in the following subsections.

5.2.1 Jet clustering

The first step in the event reconstruction is to cluster the individual energy flows of an event, trying to associate to the same jet all the particles originated in the hadronisation of the same quark (or anti-quark). In hadronic $\mathrm{W^+W^-}$ events, four primary quarks are produced and hence four jets of particles are expected. Events selected as fully hadronic $\mathrm{W^+W^-}$ candidates are thus forced to form four jets. Nevertheless, hard gluon radiation occurs in a fraction of the events, leading to five or even six jet final states. A separate treatment of these events is not considered in this analysis, but may be the source of future improvements.

Several algorithms for jet clustering exist. An important *family* of algorithms share a common procedure: a *distance* parameter, y_{ij}, is calculated between each pair of detected objects i and j. The pair with the minimum value of this parameter is combined to form a new pseudo-particle by adding the momenta. In general, this minimisation step is repeated until y_{ij} is greater than some predefined cut-off value, $\mathrm{y_{cut}}$. The pseudo-particles remaining at this stage are considered to be the jets. For the specific case of hadronic

W^+W^- events at LEP2, the procedure is slightly modified: events are forced to have four jets, by allowing variations of y_{cut}.

The distance parameter y_{ij} can be defined in many ways. Usually, it is defined as some mass variable, m_{ij}^2, scaled by the visible energy in the detector:

$$y_{ij} = \frac{m_{ij}^2}{E_{vis}^2}. \tag{5.2}$$

Different definitions of m_{ij}^2 give different clustering algorithms. For the `DURHAM` algorithm used in this analysis, the definition is

$$2\left(\min\left[E_i^2, E_j^2\right]\right)(1-\cos\theta_{ij}) \tag{5.3}$$

Several jet algorithms were tested in ALEPH, with the aim of optimising the statistical performance of the M_W measurement [101, 102]. The conclusion was that the `DURHAM` algorithm gave the better performance in terms of M_W resolution and size of the bias introduced. More specifically, a new version of the algorithm (the so-called "`PE`" *scheme*) was developed: the objects are clustered into jets assuming they are massless, and then the mass of the objects is taken into account to build the four-momenta of the jets. This is a combination of the "`P`" and "`E`" schemes that had been used in earlier experiments.

In this thesis, a new jet algorithm is introduced with the aim of reducing the QCD-related systematics. The definition of the algorithm, as well as its performance compared with `DURHAM` are given in next chapter.

Jet energy corrections

To reduce the difference between MC and data events, a correction is applied to the reconstructed MC jets to make their energy spectrum match that of the data. That is done by using either data taken at LEP1 or at some dedicated calibration runs at the Z peak during the LEP2 program. In both cases, events with two jets resulting from the fully hadronic decay of a Z boson are selected in data and MC. The energy carried by each jet should on average be equal to the LEP beam energy, E_{beam}. However, there will be some discrepancies due to the response of the detector. The ratio of the measured jet energy to the beam energy may be compared to the same ratio in data. The double ratio, R_j, gives the correction to be applied to MC jets:

$$R_j(\theta) = \frac{(E_{jet}/E_{beam})_{data}}{(E_{jet}/E_{beam})_{MC}}\,. \tag{5.4}$$

This ratio is shown in Fig. 5.2 as a function of polar angle. R should be one if data and MC were identical. Small differences between data and MC are seen, particularly in the overlap region between the barrel and end-cap calorimeters, rising to approximately 2% in the regions close to the beam pipe. To take these differences into account, any MC sample used in the analysis has its jet energies corrected by this ratio, depending upon which bin of Fig. 5.2 the jet polar angle falls.

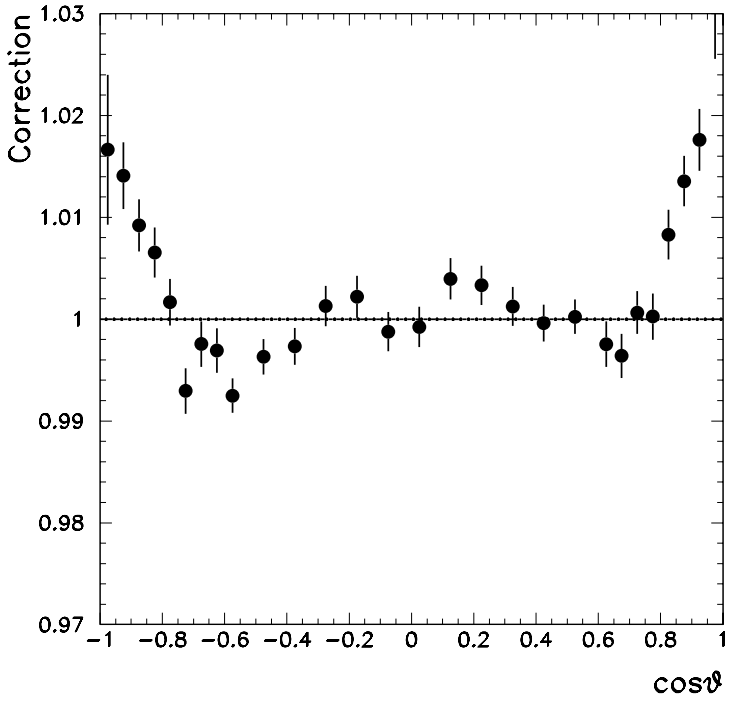

Figure 5.2: Jet corrections derived from 1994 Z data and MC as a function of jet polar angle.

5.2.2 Kinematic fitting

Since LEP is an e^+e^- collider, both the centre-of-mass energy of the event and the total momentum are precisely known. The kinematic fit exploits that information in order to improve the resolution of the jet energies and momenta and therefore the dijet invariant mass resolution.

The kinematic fit works by varying the energy and momentum of the four jets, until

the constraints of energy and momentum are satisfied:

$$\begin{aligned} \sum_{i=1}^{4} E_i &= 2E_{beam} \\ \sum_{i=1}^{4} \vec{p}_i &= \vec{0}\,. \end{aligned}$$

The variation of the four vectors is carried out by minimising an appropriate function derived from the measured and fitted four-momenta. The kinematic fitting package used in this analysis, the so-called `ABCFIT` [105], imposes the energy-momentum constraints through Lagrange multipliers, using an iterative process. The jet energy resolution is extracted from data as a function of the θ angle, and taken into account in the fitting procedure.

A relevant characteristic of the kinematic fitting is that jet energy is scaled by the same factor as the momentum, in other words the jet velocity β is not modified:

$$\beta = \frac{\left|\vec{p}_j^{\,meas}\right|}{E_j^{meas}} = \frac{\left|\vec{p}_j^{\,fit}\right|}{E_j^{fit}}\,. \tag{5.5}$$

5.3 Jet pairing

Once the kinematic fit has been performed, the four jets are paired, trying to associate those coming from the decay of the same W boson. For this analysis, the pairing algorithm chosen is based on the comparison of the `CC03` matrix element corresponding to every combination. Of the three possible pairings, the one with the largest value of the matrix element squared is selected. The element is described as:

$$\left|\mathcal{M}\left(\mathcal{M}_W^r, \Gamma_W^r, p_i^1, p_i^2, p_i^3, p_i^4,\right)\right|^2\,, \tag{5.6}$$

where M_{W}^r is a reference mass chosen to be 80.35 GeV, $\Gamma_{\mathrm{W}}{}^{\mathrm{r}}$ is the corresponding SM prediction for Γ_{W}, 2.094 GeV, and p_i^j is the four-momentum of the j-th jet.

Both masses are required to lie between 60 GeV and 110 GeV. If the first combination does not satisfy this mass window condition, the second combination is tried. If the second combination fails to pass the window requirements then the event is rejected. The combination with the largest matrix element squared is chosen in 90% of selected events and the second combination 10%. Table 5.6 summarises the performance of the pairing algorithm, as computed from MC studies.

The final number of selected and observed events is summarised in Table 5.7. The overall amount of observed events is 4.2% lower than the expectation. The discrepancy is reduced when full $\mathcal{O}(\alpha)$ electroweak corrections are included in the MC computation, as the expected cross-section decreases by a 2.4% (see Ref. [106] for a discussion). The preliminary measurement of the W^+W^- pair production cross-section by ALEPH gives a value that is lower than the corrected prediction by ∼1%, corresponding to approximately one standard deviation [107]

$\sqrt{s}$ (GeV)	Events in window (true pairing)	Efficiency	Purity
189	99.8%	79.6%	89.6%
207	99.8%	77.3%	90.5%

Table 5.6: Performance of the pairing algorithm. The first column shows the fraction of events that satisfy the mass window cut when the true pairing is applied. The efficiency of the pairing in the next column is computed with respect to that subsample of events. The purity is defined as the fraction of events where the right pairing is found.

$\sqrt{s}$ (GeV)	Events Expected	Events Observed
183	420	450
189	1349	1240
192	226	250
196	643	613
200	699	657
202	338	297
205	664	633
207	1082	1054

Table 5.7: Expected and observed number of selected events at each $\sqrt{s}$.

5.4 Invariant mass distribution

After the reconstruction of the events, a final invariant mass distribution is obtained. Fig. 5.3 shows a comparison of this distribution at $\sqrt{s} = 207\,\text{GeV}$ for data and MC. The

later has been generated with an input M_{W} of 80.35 GeV, and it has been reweighted to fit the distribution of data. M_{W} is actually extracted from the two dimensional distribution obtained when the masses of the two W bosons of the events are taken into account.

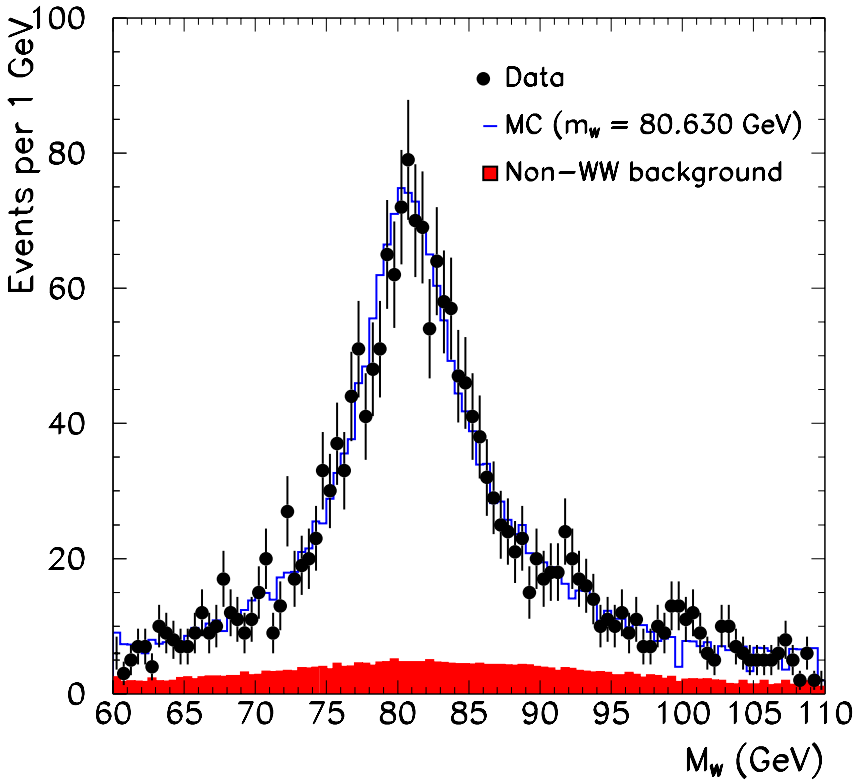

Figure 5.3: Reconstructed mass distribution for the $\sqrt{s}$ = 207 GeV data and MC. The $\mathrm{W^+W^-}$ MC has been generated with an input mass of 80.35 GeV and reweighted to fit the data distribution.

Chapter 6

W mass extraction

Once the event by event invariant masses are built, the underlying M_{W} has to be extracted. The first section of this chapter reviews the different extraction methods used at LEP. Afterwards, the reweighting method used in this thesis is described, as well as some of the technicalities of the fitting procedure.

6.1 Mass extraction methods

Different techniques for extracting the M_{W} from the reconstructed dijet invariant mass distribution have been tested by the LEP collaborations. A brief description of three of them follows.

(i) **Breit-Wigner Fit:** An analytical function such as a double Breit-Wigner is used to fit the invariant mass distribution. In general, the fitted function will not be able to describe the experimental distribution perfectly due to effects such as initial state radiation, background contamination and detector resolution. This fact leads to a loss of sensitivity, as well as to a bias in the fitted M_{W} which must be corrected for. MC samples generated at several different M_{W} values are treated as data and their mass distributions fitted to obtain a calibration curve. Any discrepancy between MC and data will translate into a systematic uncertainty through this calibration. The fact that the fitting function is not the underlying experimental distribution makes it impossible to compute exactly the statistical uncertainty [108].

(ii) **Convolution:** The convolution method is an extension of the simple Breit-Wigner fit that takes into account the detector response. An analytical function describing

the underlying physics of the event is convoluted with a function describing the detector resolution on an event by event basis. Generally, the physics function is more complete than a simple Breit-Wigner, and it is often the differential cross-section in terms of the two invariant masses, usually including an ISR description. This method uses a lot of computation time, making stability and systematic checks difficult. In particular, the CPU time needed for studies on systematic uncertainties related to the detector makes the method unpractical.

(iii) **MC Interpolation:** A large number of MC samples is generated at different values of M_{W}. The event selection and invariant mass reconstruction is carried out for each of these samples in order to obtain an invariant mass distribution that can be directly compared with that obtained from the data. A quantity that describes how well the data distribution fits the different MC distributions is constructed and then the best estimate for the fitted M_{W} is obtained by interpolation between the mass points. This method has the advantage that MC and data events are treated in exactly the same way, hence no calibration is needed. The major disadvantage of this method is the huge number of MC events needed.

6.2 The MC reweighting method

The method used in this analysis follows from the MC interpolation method, but the technique of reweighting removes the need for many different samples of MC events.

A large sample of MC events are generated at a reference M_{W}, and the invariant mass distribution is obtained in the same way as for the data. The reweighting technique consists in modifying the distribution to obtain that corresponding to a different mass. The reweighting is carried out on an event-by-event basis. The weight corresponds to the ratio of the squares of the `CC03` matrix elements for the event with the modified and the reference mass:

$$w_i\left(M_W^0, \Gamma_W^{ref}\right) = \frac{\left|\mathcal{M}\left(M_W^0, \Gamma_W^{ref}, p_i^1, p_i^2, p_i^3, p_i^4,\right)\right|^2}{\left|\mathcal{M}\left((M_W^{ref}, \Gamma_W^{ref}, p_i^1, p_i^2, p_i^3, p_i^4,\right)\right|^2}, \tag{6.1}$$

Previous studies [101] have shown that the effect on the fitted mass of using the `CC03` matrix element instead of the full four fermion matrix element is negligible, while

it takes much less computation time. In order to speed up even more the procedure, reweighted distributions are produced only at masses with a separation of 25 MeV. A linear interpolation is performed to intermediate masses. This interpolation has a negligible effect on the fitted M_{W}.

6.2.1 Construction of the probability density function

The statistical precision of the measurement is improved by using a two dimensional mass distribution to perform the fit. The two dimensions correspond to the two reconstructed masses obtained after the 4C kinematic fit and jet pairing procedure. The improvement in the statistical precision arises because the mass-to-mass correlations in each event are taken into account. At $\sqrt{s} = 183\,\mathrm{GeV}$, the improvement in the expected precision of the measurement was 10% [101] with respect to the result from a one-dimensional fit.

The invariant mass distribution of the MC reference is the sum of the contributions of signal and background, each binned separately. Each event gives a single point on the two dimensional mass plane (M_1, M_2). The probability density function for a data event to have a particular invariant mass coordinate is then taken as the sum of the signal and background distributions.

The $\mathrm{W^+W^-}$ cross-section depends on M_{W} and so this dependence has to be included in the probability density function to ensure the correct signal to background normalisation. In the region where the fit is performed the variation is small and is parametrised with a parabola around $M_W^0 - M_W^{ref}$. The parabola has the form $\sigma_s\left(M_W^0\right) = \sigma_s\left(M_W^{ref}\right)\left(1 + a\left(M_W^0 - M_W^{ref}\right) + b\left(M_W^0 - M_W^{ref}\right)^2\right)$, and is determined using the `GENTLE` package [110].

The variation of the $\mathrm{W^+W^-}$ cross-section with M_{W} is shown in Fig. 6.1, for two values of the centre-of-mass energy. The efficiencies are determined from MC and are assumed to have no dependence on M_{W}.

6.2.2 Binning of the probability density function

The probability density function (p.d.f.) is binned separately for signal and background. The binning must be carefully chosen in order to minimise any possible bias due to the finite number of MC events used, while maximising the sensitivity to M_{W}. Previous

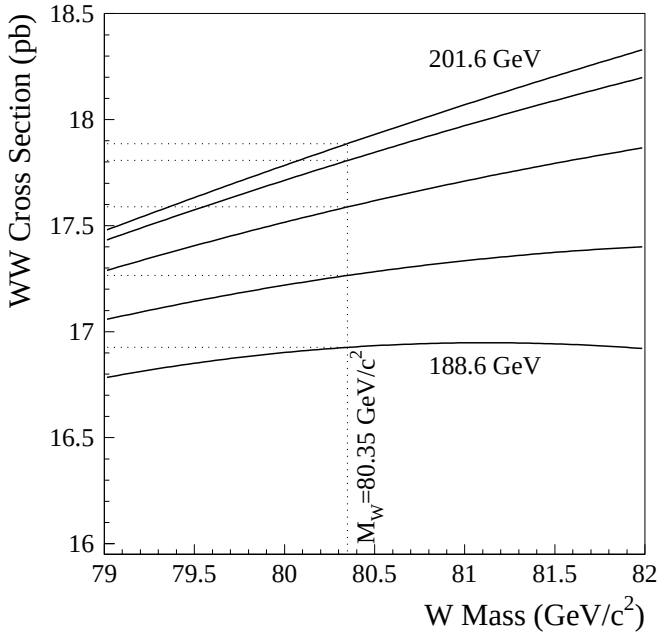

Figure 6.1: The parametrisation of the W^+W^- cross section as a function of M_W, for $\sqrt{s}$ = 189 GeV (bottom curve), 192, 196, 200 and 202 GeV (top curve).

studies [101] show that the optimal solution is the use of a variable bin size, demanding a minimum number of events in each bin (N_{ij}^{min}).

If N_{ij}^{min} is too large, sensitivity is lost, while if it is too small the measurement becomes biased towards the reference mass used in the MC, unless the proper uncertainty is taken into account. The optimal value is found to be $N_{ij}^{min} \sim 200$ [102].

6.2.3 Maximisation of likelihood

To find the best estimate of M_W, the probability density function obtained in the previous section is used to construct a likelihood function. The function depends upon the reconstructed invariant masses for each data event and the value of M_W to which the MC was reweighted (M_W^0):

$$\mathcal{L}\left(M_W\right) = \prod_{i=1}^{N_{evt}} pdf_{data}\left(M_1^i, M_2^i | M_W^0\right) \ . \tag{6.2}$$

N_{evt} is the number of data events. This likelihood is then maximised to find the fitted value of M_{W}. In practice, the quantity $-2\ln\mathcal{L}$ is minimised using the `MINUIT` package [111].

The statistical uncertainty on the fitted M_{W} is taken as the 68% confidence level region, corresponding to one standard deviation of a Gaussian distribution. In the limit of large sample sizes the logarithm of the likelihood is a parabola, with the minimum of $-2\ln\mathcal{L}$ at the fitted M_{W}. The statistical uncertainty may then be calculated analytically by inverting the second derivative of $\ln\mathcal{L}$. In practice the 68% confidence level region is determined numerically, its boundaries occurring when $-2\ln\mathcal{L}$ is one unit greater than at its minimum.

This calculation of the fit uncertainty assumes that the response of the analysis to the true M_{W} is linear.

6.3 Monte Carlo Studies

6.3.1 Expected statistical uncertainty

MC studies allow to test whether the fit uncertainty correctly estimates the statistical uncertainty on M_{W}. Subsamples of MC of the the size of the data sample can be made, and M_{W} fitted for each of them. The expected uncertainty, corresponding to the r.m.s. of the distribution of values obtained, has been checked to be consistent with the fit uncertainty [104].

6.3.2 Linearity check

As explained in Section 6.2, the method of reweighting is not expected to need calibration. The analysis should therefore have a linear response: the fitted mass should reproduce the true mass when it has a different value from the M_{W} used as input to the MC reference. This has been tested using five samples of MC, each generated at different input W masses between 79.85 GeV and 80.85 GeV (200K of events each). A straight line fit shows that the analysis is indeed linear (Fig. 6.2), with no bias within the MC statistical uncertainty.

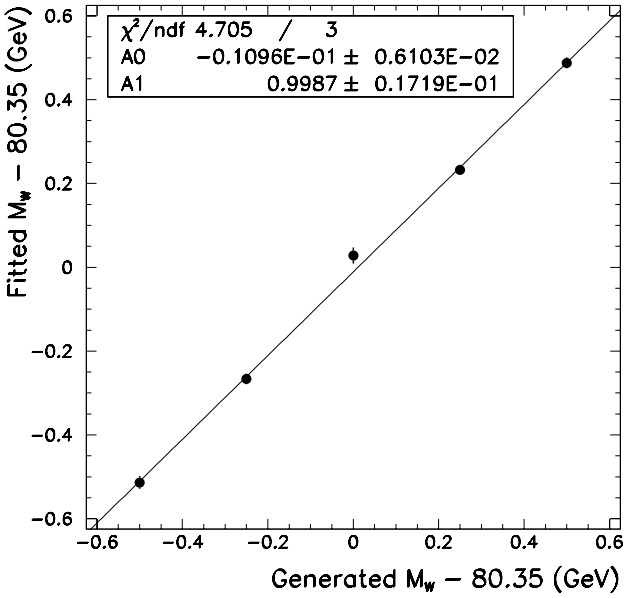

Figure 6.2: The fitted M_{W} versus the generated M_{W}. The result of a straight line fit to the points is shown as a solid line and the values of the offset (A0) and the slope (A1) are given in the plot, together with the χ^2 of the fit. The fit is compatible with a straight line with no offset and slope equal to unity.

6.4 Data fit results

The results of the fit to the LEP2 data samples are shown in Table 6.1, together with the statistical uncertainty from the fit and that expected from the number of observed events. The fitted masses have had 27 MeV added to them to account for the difference in the running width and fixed width schemes as explained in Section 2.3. The observed uncertainty on the fitted mass is quoted as the mean of the positive and negative fit uncertainties.

The stability of the measurement under modifications of every step of the selection and reconstruction processes has been checked extensively in previous studies [104]. In particular, the measurement has been proven to be stable when the value of the cut on the NN output is varied as well as when the values of the mass window are modified.

$\sqrt{s}$ (GeV)	Fitted Mass (GeV)	Statistical uncertainty (GeV)	Expected uncertainty (GeV)
183	80.472	0.185	0.167
189	80.553	0.106	0.106
192	80.258	0.252	0.204
196	80.505	0.147	0.156
200	80.223	0.158	0.122
202	80.457	0.241	0.178
205	80.502	0.140	0.150
207	80.657	0.118	0.116

Table 6.1: Results of the fit for the W mass from data, showing the observed and expected statistical uncertainties for observed number of events.